sensors

MDPI

Article

ZnO Doped Silica Nanoparticles ($ZnO@SiO_2$) for Enhanced Electrochemical Detection of Cd^{2+} Ions in Real Samples

Afef Dhaffouli [1,2], Michael Holzinger [3], Soledad Carinelli [4], Houcine Barhoumi [1] and Pedro A. Salazar-Carballo [4,*]

[1] Laboratory of Interfaces and Advanced Materials, Faculty of Sciences of Monastir, University of Monastir, Monastir 5000, Tunisia; dhaffouliafef@gmail.com (A.D.); houcine.barhoumi@fsm.rnu.tn (H.B.)
[2] Department of Chemistry, Faculty of Sciences of Gafsa, University of Gafsa, Gafsa 2100, Tunisia
[3] Department of Molecular Chemistry UMR CNRS 5250, Grenoble-Alpes University, CEDEX 9, 38058 Grenoble, France; michael.holzinger@univ-grenoble-alpes.fr
[4] Laboratory of Sensors, Biosensors and Advanced Materials, Faculty of Health Sciences, University of La Laguna, Campus de Ofra s/n, 38071 La Laguna, Spain; scarinel@ull.edu.es
* Correspondence: psalazar@ull.edu.es; Tel.: +34-922-319422

Abstract: Pollution by heavy metal ions has a serious impact on human health and the environment, which is why the monitoring of heavy metal ions is of great practical importance. In this work, we describe the development of an electrochemical sensor for the detection of cadmium (Cd^{2+}) involving the doping of porous SiO_2 spheres with ZnO nanoparticles. Zinc oxide is chosen as the central dopant in the composite material to increase the conductivity and thus improve the electrochemical detection of Cd^{2+} ions with the SiO_2 spheres. The resulting composite is characterized by electrochemical spectroscopic XRD and microscopic methods. As a result, the developed sensor shows good selectivity towards the targeted Cd^{2+} ions compared to other divalent ions. After optimization of the experimental conditions, the electrochemical sensor shows two different linear ranges between 2.5×10^{-11} molL^{-1} to 1.75×10^{-10} molL^{-1} and 2×10^{-9} molL^{-1} to 1.75×10^{-9} molL^{-1}, indicating a change from diffusion-controlled to surface-controlled oxidation of Cd^{2+}. A detection limit was reached at 4.4×10^{-11} molL^{-1}. In addition, it offers good repeatability and recovery, and can detect accurate trace amounts of Cd^{2+} ions in real samples such as tap water or seawater by spiking these samples with known Cd^{2+} concentrations. This setup also provides satisfactory recovery rates in the range of 89–102%.

Keywords: electrochemical sensor; Zinc oxide; Porous silica coating; Cd^{2+} detection; $ZnO@SiO_2$ NPs

Citation: Dhaffouli, A.; Holzinger, M.; Carinelli, S.; Barhoumi, H.; Salazar-Carballo, P.A. ZnO Doped Silica Nanoparticles ($ZnO@SiO_2$) for Enhanced Electrochemical Detection of Cd^{2+} Ions in Real Samples. *Sensors* **2024**, *24*, 4179. https://doi.org/10.3390/s24134179

Academic Editor: Raluca-Ioana Stefan-van Staden

Received: 29 May 2024
Revised: 21 June 2024
Accepted: 24 June 2024
Published: 27 June 2024

1. Introduction

Cadmium is present in the environment in elemental form or as various salts that enter drinking water sources through natural processes (leaching from the soil), human activities (product refinement or technological applications), or leaching from certain types of pipes and known components [1]. This not only affects the health of humans, animals, and plants, but also the ability of the environment to sustain life. As heavy metals are not biodegradable, they accumulate in the food chain. According to the World Health Organization (WHO) [2], a heavy metal concentration above the permissible limit can be toxic, carcinogenic, and harmful to human health [3]. Their high water solubility facilitates their spread in the environment and leads to environmental pollution [4]. The maximum level of Cd^{2+} ions in drinking water is 3.0 μgL^{-1}, according to US Environmental Protection Agency (USEPA) standards [5]. It accumulates in humans, reacts with enzymes, and generates free radicals [6], leading to serious health problems. Recent studies have classified Cd^{2+} as a type I human carcinogen [7]. Therefore, the reliable detection of Cd^{2+} is of utmost importance. Effective methods for the determination of Cd^{2+} ions require high selectivity and sensitivity [8]. Various methods are used for the detection of heavy metal

ions, which are divided into three classes: electrochemical [9–11], gravimetric [12,13], and optical detection methods [14].

However, despite the excellent sensitivity and selectivity achieved with these techniques, sophisticated instrumentation and competent personnel for careful sample preparation are unsuitable for on-site screening [15–17]. Among the recently developed technologies for Cd^{2+} detection, electrochemical sensors are considered economical because the equipment and operating procedures are generally simpler and less expensive than other technologies [18]. In addition, electrochemical sensors have many advantages, including being cheap, portable (in situ real-time detection), simple, and offering higher sensitivity and specificity than the detection methods already mentioned [19–21]. It has been found that that nanocomposites are core components and play an important role in the development of sensitive electrochemical Cd^{2+} sensors. Electrochemical methods are widely used due to their low cost, simple equipment, easy operation, and strong anti-interference capabilities [22,23]. To improve the sensitivity of the electrochemical sensor, various chemically modified electrodes with nanomaterials [24], magnetic substances [25,26], automotive materials [27], and biological composites [28] have been used. However, these methods are limited in their ability to specifically detect Cd^{2+} ions. Although silica nanoparticles (NP) are an electronic insulator, they are widely used in electrochemical analysis due to their large effective surface area with high selectivity and good sensitivity to heavy metal ions [29–32].

In this work, a sensitive and selective electrochemical sensor based on ZnO@SiO_2 was fabricated for the detection of Cd^{2+} ions in real samples. First, these particles were prepared by a modified sol-gel method in the presence of tetraethyl orthosilicate (TEOS). In this technique, a layer of silicon dioxide spheres is formed around the ZnO particles at a controlled temperature of 40 °C. The electrochemical performance of the fabricated sensors was investigated under optimized experimental conditions. The results showed that these sensors were very sensitive to Cd^{2+} ions. Furthermore, by comparing the response current of the electrochemical sensor with other metal ions using differential pulse voltammetry (DPV), it was proven that the sensor exhibited increased signal performance for Cd^{2+} ions. The sensor was also tested on real samples, with deviations ranging from 89 to 102% regarding the spiked Cd^{2+} concentration as 100%.

2. Materials and Methods

2.1. Materials and Reagents

Zinc oxide nanoparticles (ZnO NPs, nanopowder with a particle size < 100 nm), tetraethyl orthosilicate (TEOS), and ethanol (EtOH) were sourced from Sigma-Aldrich. Sodium hydroxide (NaOH), potassium hexacyanoferrate (II) trihydrate ($K_4[Fe(CN)_6]\cdot 3H_2O$), potassium hexacyanoferrate (III) ($K_3[Fe(CN)_6]$), potassium chloride (KCl), copper (II) dichloride ($CuCl_2$), lead nitrate ($Pb(NO_3)_2$), cadmium nitrate ($Cd(NO_3)_2\cdot 4H_2O$), nickel (II) dichloride hexahydrate ($NiCl_2\cdot 6H_2O$), manganese (II) dichloride tetrahydrate ($MnCl_2\cdot 4H_2O$), and iron (II) dichloride ($FeCl_2$) were acquired from Sigma-Aldrich through Chimisi and Chimie Tunisie companies (Tunisia). Acetate buffer solution (ABS, 0.1 $molL^{-1}$; pH 5) was formulated by mixing a 0.1 $molL^{-1}$ acetic acid solution (CH_3COOH, HAc) and a 0.1 $molL^{-1}$ sodium acetate solution (CH_3COONa; NaAc) in a 1:1 ratio. This ABS served as the supporting electrolyte, with pH adjustment achieved by incorporating solutions of NaOH or HCl.

Varied concentrations of copper (II), lead (II), nickel (II), manganese (II), iron (II), and cadmium (II) were prepared in an acetate buffer solution (ABS) using distillated water. A stock solution of Cd^{2+} was diluted until the desired trace concentrations were obtained. For each dilution, the solutions were stirred until stabilization of the corresponding concentration. The experiments for the detection of Cd^{2+} concentrations were performed using firstly the lowest concentration followed by the higher concentration.

2.2. Preparation of ZnO@SiO2

In this step, 0.5 g ZnO nanoparticles were dispersed in 50 mL ethanol and 10 mL water for 30 min in an ultrasonic bath. Then 1.6 mL of ammonia solution (1 molL^{-1}) and 8 mL of TEOS were successively added to the Zinc oxide dispersion with vigorous stirring for 6 h at 40 °C. The mixture was washed three times with ethanol and distilled water and finally dried in an oven at 60 °C for 12 h (Figure 1).

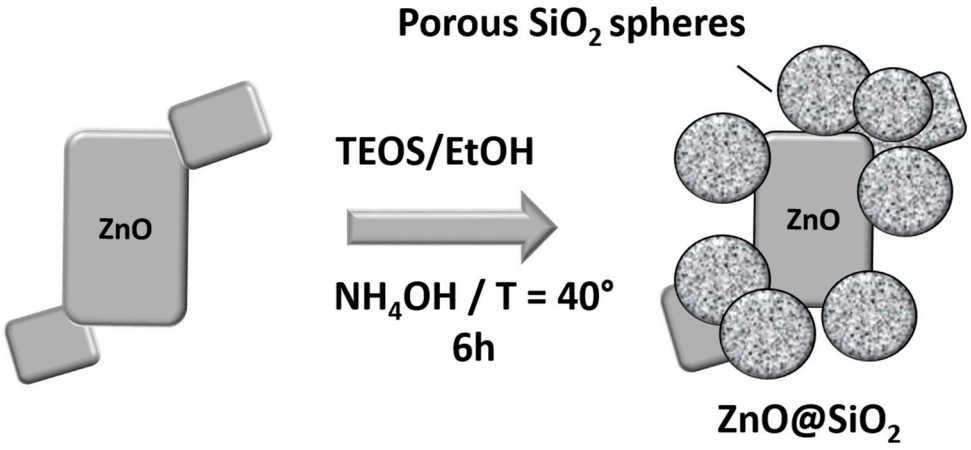

Figure 1. Schematic illustration of the formation of the ZnO@SiO_2 nanocomposite.

2.3. Fabrication of ZnO@SiO_2/GCE Modified Electrodes

Before each use, glassy carbon electrodes (GCE, Ø = 3 mm) were polished with 0.05 μm aluminum oxide powder using emery paper, rinsed with distilled water, and then ultrasonically cleaned in ethanol for 5 min to obtain a reproducible condition. After cleaning the electrode, 1 mg of ZnO@SiO_2 was dispersed in 1 mL of ethanol by sonication for 30 min and then 3 to 20 μL of the suspension was applied to the GCE. The modified electrodes were then dried at room temperature before being used for measurements.

2.4. Characterization of As-Prepared Samples

The morphologies and microstructures of the samples were analyzed by scanning electron microscopy (SEM) using a JEOL JEM-2100 FX microscope (JEOL Ltd., Tokyo, Japan). Transmission electron microscopy (TEM) images were obtained using a JEOL 2100 microscope at 200 kV (JEOL Ltd., Tokyo, Japan). X-ray diffraction patterns for powder samples were obtained with a Philips PanalyticalX'Pert powder diffractometer using CuKα (λ = 1540 Å) radiation in the 2θ range from 5° to 80°. Infrared (IR) spectra were recorded using a PerkinElmer Spectrum IR version 10.6.2 spectrometer and ultraviolet-visible spectroscopy was performed using a Beckman DU640 UV/Vis to further characterize the samples. Electrochemical measurements were performed with a computer-controlled Au-tolab PG Potentiostat/Galvanostat (AUT 83965) and controlled by Autolab's NOVA 2.1.6 software (Metrohm, Switzerland). The measurements were performed in a traditional three-electrode cell configuration. The working electrode consisted of a modified GCE, while a platinum wire served as the counter electrode and Ag/AgCl (3 molL^{-1} KCl) as the reference electrode. In brief, Cd^{2+} ions were detected using differential pulse voltammetry (DPV). For this purpose, the Cd^{2+} ions were first reduced and accumulated on the sensor surface at −1 V vs. Ag/AgCl for 5 min. Subsequently, a potential sweep from −1 to −0.4 V was applied to detect the target species under optimized conditions (see Supplementary Data).

3. Results

3.1. Material Characterization

3.1.1. Morphology and Structure of ZnO@SiO_2

The chemical nature and phase composition of the ZnO@SiO_2 nanocomposite were analyzed using the XRD technique. The main peaks in the experimental diffractogram are shown in Figure 2. The characteristic peaks at 2θ = 31.76°, 34.41°, 36.25°, 47.53°, 56.59°, 62.85°, 66.37°, 67.94°, 69.08°, and 76.95° observed in the XRD diffractogram were assigned to planes (100), (002), (101), (102), (110), (103), (200), (112), (201), and (202), respectively. These results confirm the existence of ZnO with a hexagonal wurtzite phase (space group: P63mc, JCPDS Chart No. 01-079-2205). The XRD pattern for SiO_2 shows a characteristic broad band centered at about 2θ = 23° associated with the amorphous phase of silica. This broad band is due to the phenomenon of diffuse scattering often observed in amorphous materials. The diffractogram of the ZnO@SiO_2 configuration showed that the crystal structure of ZnO was not affected by the presence of SiO_2 [33]. This can be attributed to the good dispersion of the ZnO nanoparticles in the SiO_2 matrix [34]. These results are in agreement with our previous studies [35,36].

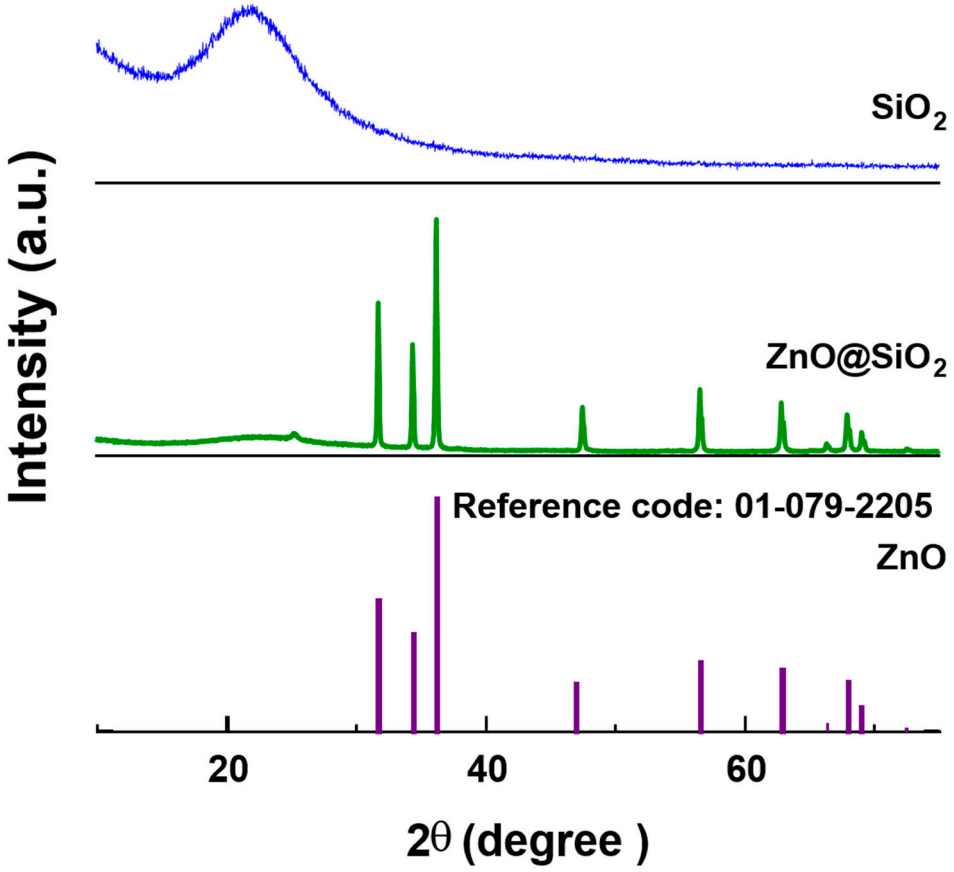

Figure 2. XRD patterns of SiO_2, ZnO@SiO_2, and the reference pattern of ZnO (01-079-2205).

3.1.2. Electron Microscopy Analysis

In general, the morphology of almost all metal oxide composites (MO@SiO_2) tends to form agglomerates of nanoparticles [37]. Figure 3a shows the scanning electron microscopy (SEM) images of commercial ZnO NPs. The particles have a cubic shape and a rather large size distribution between 100 nm and several micrometers. Figure 3b shows the synthesized SiO_2 spheres with an average size of 250 nm. The inset is a magnification of the micrograph to reveal the porous, almost fuzzy, morphology of the NP surface. Figure 3c is a representative SEM image of the ZnO@SiO_2 composite. The ZnO particles are mainly covered by the SiO_2 spheres and only a few ZnO particles with a SiO_2 coating can be seen.

Figure 3d–f are TEM images of ZnO particles, SiO_2 spheres, and the ZnO@SiO_2 composite, respectively. ZnO consists of agglomerates of particles with a broad size distribution, which explains the need for ultrasound to disperse these particles. The SiO_2 spheres also form agglomerates, in which the cross-linked SiO_2 is clearly visible in the TEM image. The ZnO@SiO_2 composite forms denser clusters of SiO_2 spheres around the ZnO particle. However, the formation of a SiO_2 layer on the ZnO particles is not clearly visible in this microscopic study.

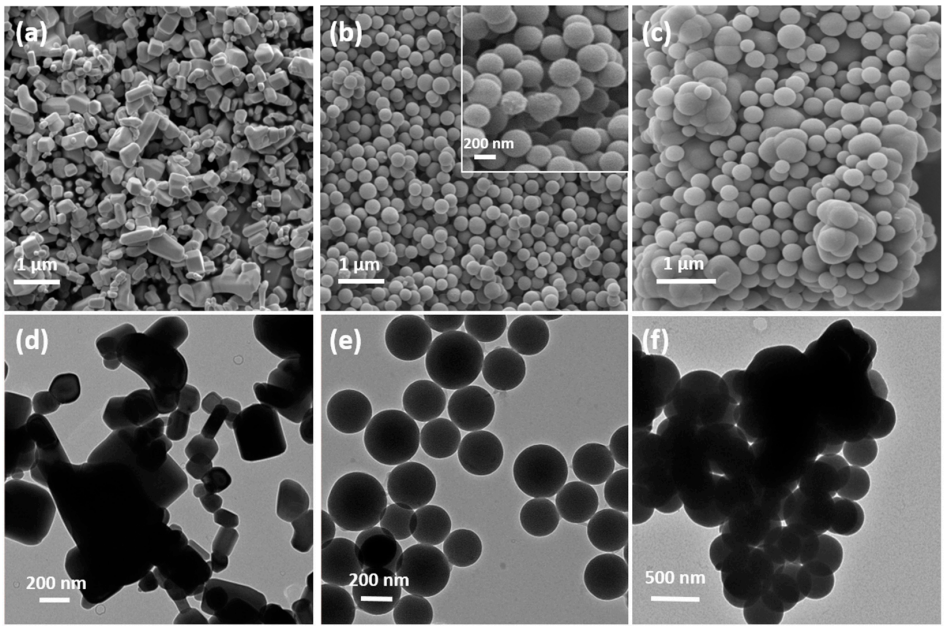

Figure 3. SEM image of (**a**) commercial ZnO NPs, (**b**) synthesized SiO_2 NPs with a zoom inset, and (**c**) ZnO@SiO_2.agglomerates. Representative TEM images of (**d**) commercial ZnO NPs, (**e**) synthesized SiO_2 NPs, and (**f**) ZnO@SiO_2.

3.1.3. Characterization of the Prepared Materials by Infrared Spectroscopy

Figure 4 shows the FTIR spectra of ZnO, SiO_2, and ZnO@SiO_2 samples. Absorption bands at 451, 794, and 1065 cm^{-1} are observed for the SiO_2 nanoparticles. These bands are close to the bands described in the literature [38] (466, 808, and 1100 cm^{-1}) and are consistent with the SiO_2 bonding structure. The band corresponds to the symmetric stretching vibration between Si-O bonds of Si-O-Si [39]. Changes in the band characteristics of SiO_2 indicate that O-Si-O is perturbed by the presence of oxides in its environment. Studies show that in a mixed crystal, the substitution or filling of vacancies can lead to a shift in the fundamental transverse optical modes. The ZnO spectrum shows only one strong absorption peak at 359 cm^{-1}. This is the characteristic band of the monoclinic phase of pure Zn-O [40]. The band at 3300 cm^{-1} in the SiO_2 and ZnO@SiO_2 spectra indicates the presence of water, which is due to moisture absorption from the environment, the -OH stretching vibration of H_2O, and the -OH stretching vibration of Si-OH. In addition to the characteristic peaks of ZnO and SiO_2, the spectrum of ZnO@SiO_2 samples exhibits another small absorption peak at 556 cm^{-1}, which is due to the formation of some Si-O-Zn bonds. These results are in agreement with the results of FTIR studies in the literature [41,42].

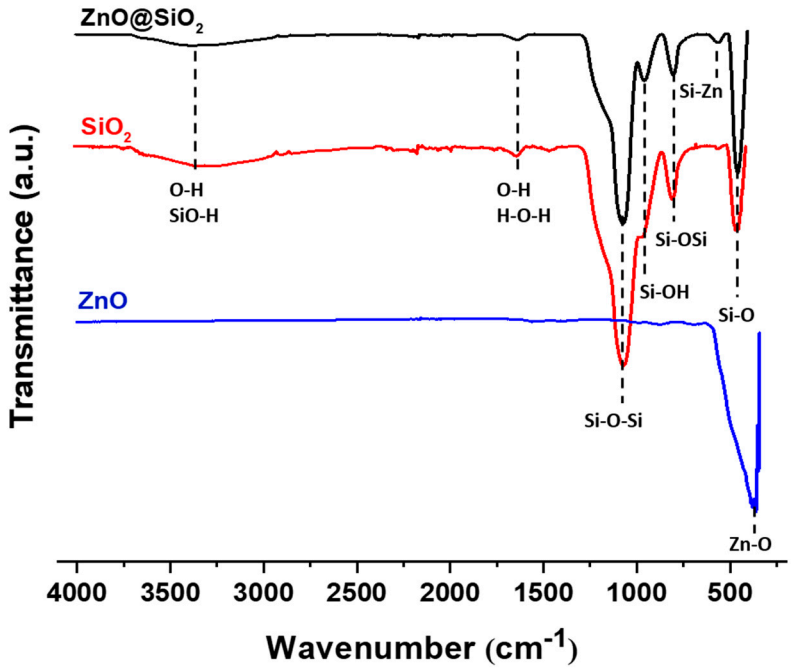

Figure 4. FT-IR spectra of ZnO, SiO_2, and ZnO@SiO_2 NPs.

3.1.4. UV–Vis Spectra

Figure 5 shows the UV-Vis absorption spectra of ZnO, SiO_2, and ZnO@SiO_2, measured in the wavelength range between 228 nm and 400 nm. In contrast to the spectra of ZnO@SiO_2 and ZnO, the spectrum of the pure SiO_2 spheres does not show a clearly resolved absorption band, which confirms that the band found in the spectrum of ZnO@SiO_2 corresponds to the ZnO in the composite. The spectrum of ZnO@SiO_2 shows a clear band between 240 nm and 300 nm, while the band of ZnO@SiO_2 appears to be broader, indicating an increase in the transition levels due to the SiO_2 spheres bound to the ZnO [43]. In a similar study on a CaO@SiO_2 nanocomposite, the maximum absorption wavelength was reported to be 300 nm [44], which is consistent with the optical properties of the present study. The narrow bandwidth at 270 nm is the result of small ZnO nanoparticles remaining in the porous silica structure [38,45].

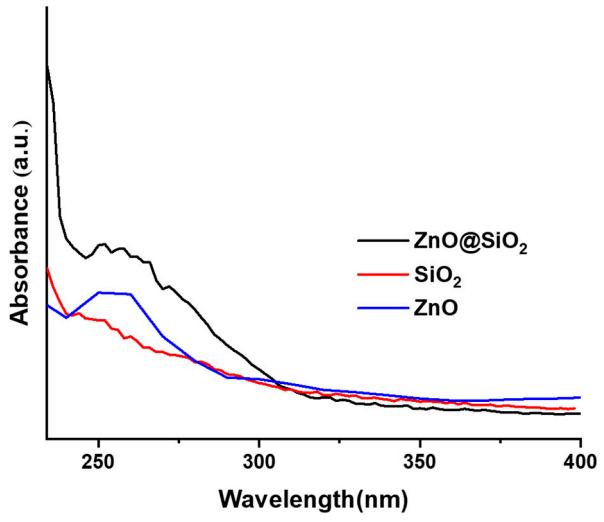

Figure 5. UV–Vis spectra for samples of SiO_2 and ZnO@SiO_2.

3.2. Electrochemical Studies

3.2.1. Optimization of Experimental Variables

To evaluate the effect of different parameters for the detection of Cd^{2+} with $ZnO@SiO_2$ modified electrodes, we determined the optimal conditions, such as the amount of composite, drying time, pH, and accumulation time. As for the amount, different volumes (3 µL to 20 µL) of $ZnO@SiO_2$ solution (1 mg mL^{-1} in ethanol) were applied to the GCE surface, and the highest DPV signal was obtained at 7 µL (Figure S1a). Higher amounts obviously passivate the electrode, which is due to the insulating character of SiO_2, despite the ZnO doping. We also observed that the drying time of the composite significantly affects the sensor performance. At a drying time of 2 h, the response current reaches its maximum, and at more than 2 h, the response current decreases significantly (Figure S1b). This decrease in current can be explained by the fact that our $ZnO@SiO_2$ layer requires a certain amount of moisture to interact sufficiently with the Cd^{2+} ions. If it is too dry, the $ZnO@SiO_2$ becomes hydrophobic and the pores are not properly filled by the analyte solutions. To investigate the effects of pH on the response of the electrode, DPV experiments were performed in the pH range from 3 to 8, as shown in Figure S1c. An increase in pH from 3.0 to 5.0 leads to an increase in peak current at −0.78 V vs. Ag/AgCl, with the maximum intensity for Cd^{2+} ions being reached at pH 5.0. Subsequently, the peak currents decreased with increasing pH values. At a mildly acidic pH value, Cd^{2+} is completely ionized, while at higher pH values hydroxides are formed which impair the oxidation capacity of the Cd^{2+} ions. Conversely, at lower pH values (approx. < 4) protons can compete with Cd^{2+} ions for the binding sites.

Finally, the effect of incubation time on peak current intensity was investigated between 1 and 10 min in a 0.1 $molL^{-1}$ acetate buffer solution at pH 5.0 containing 10^{-9} $molL^{-1}$ Cd^{2+}. Figure S1d shows that the current increases with increasing accumulation time from 1 min to 5 min, which can be attributed to the significant increase in the oxidation of the metal ions on the $ZnO@SiO_2$/GCE surface. These results confirm that the $ZnO@SiO_2$ nanoparticles have a good ability to rapidly accumulate the analyte due to their large active surface area. After 5 min at −1 V vs. Ag/AgCl, the intensity of the current peak decreased. The accumulation time and potential serves to reduce the captured Cd^{2+} ions to Cd^0, which are then re-oxidized to Cd^{2+} during the DPV measurements. Longer accumulation times had no positive effect on the response, indicating that the electrode surface had reached saturation of the Cd^{2+} that can be reduced and oxidized. Figure 6 illustrates the capture and adsorption of Cd^{2+} ions on the surface bound silanol (Si-OH) functions, most likely via dominant polar interactions because at pH 5 these functions can be considered as completely protonated. These ions are reduced to $Cd^{(0)}$ during accumulation and concentration at −1.0 V vs. Ag/AgCl. It is further shown that the pathways of electrons are mediated via the ZnO particles to the SiO_2 shell. During reverse potential scanning using DPV, $Cd^{(0)}$ is re-oxidized to Cd^{2+}, giving the electrochemical signal.

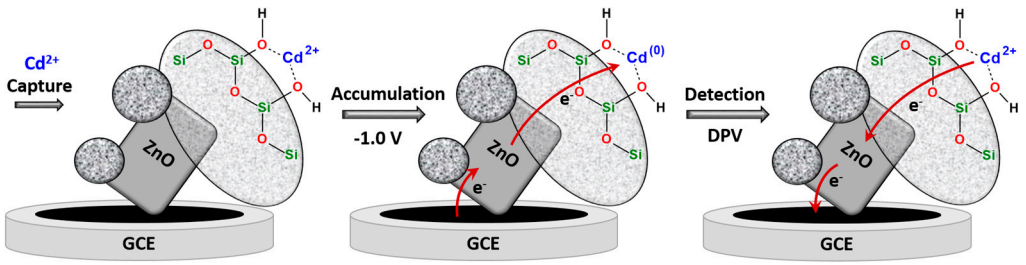

Figure 6. Schematic representation of the adsorption of Cd^{2+} ion of the SiO_2 surface via polar interactions, the formation of $Cd^{(0)}$ during accumulation via ZnO mediated electron transfers, and reformation of Cd^{2+} during DPV measurements.

3.2.2. Detection of Cd^{2+}

After optimizing the experimental parameters, we investigated the ability of the $ZnO@SiO_2$-modified GCE as an electrochemical sensor for the detection of Cd^{2+} ions in

aqueous solutions. The DPVs of a bare GCE, SiO_2/GCE, and ZnO@SiO_2/GCE electrodes were recorded in a 0.1 molL^{-1} ABS (pH = 5:0) solution containing 1.75 × 10^{-9} molL^{-1} Cd^{2+} (Figure 7). No obvious response was observed for the bare GCE and ZnO-modified electrode when the accumulation time was 5 min. A small peak with an oxidation current of 1.3 µA was observed for the SiO_2-modified electrode, which is much lower compared to the ZnO@SiO_2-modified electrode, which showed a strong reaction peak at −0.78 V vs. Ag/AgCl with a peak current Ipeak = 4.75 µA. This significant difference can be attributed to the insulating nature of SiO_2, which prevents signal trapping for Cd^{2+} detection. Doping with conductive ZnO particles significantly improves the electron transfer between the electrode and the trapped Cd^{2+} ions.

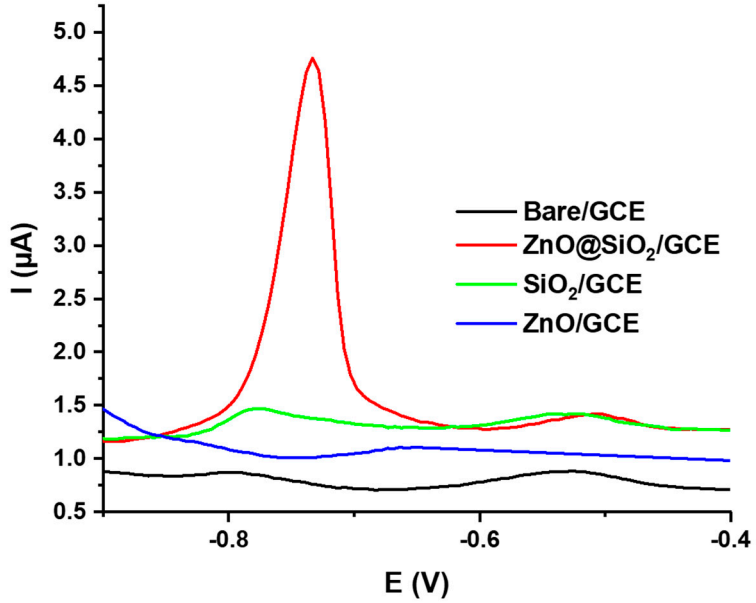

Figure 7. DPV results of bare GCE, SiO_2/GCE, ZnO/GCE, and ZnO@SiO_2/GCE electrodes measured in 1.75 × 10^{-9} molL^{-1} Cd^{2+}. Data were recorded after drop casting 7 µL of a 1 mg mL^{-1} ZnO@SiO_2 solution in ethanol, a drying time of 2 h, and an accumulation time of 5 min in 0.1 molL^{-1} in ABS buffer at pH 5.

This observation proves the suitability of ZnO@SiO_2 as a sensitive layer for the electrochemical detection of Cd^{2+} ions. Figure 8a shows the DPV responses of ZnO@SiO_2/GCE at different Cd_{2+} concentrations. After baseline correction for each DPV, the resulting calibration curve (Figure 8b) shows two linear regions, with linearity values of R^2 = 0.993 for low concentrations and R^2 = 0.986 for higher concentrations. These two linearities can be attributed to the change in the electrochemical Cd^{2+} oxidation from diffusion-controlled domain at lower concentrations (from 2.5 × 10^{-11} molL^{-1} to 1.75 × 10^{-10} molL^{-1}) and to surface-controlled processes at higher concentrations (from 2 × 10^{-10} molL^{-1} to 1.75 × 10^{-9} molL^{-1}). The linearity is not perfect, but satisfying considering the overall low concentration range. At higher concentrations, the electrode surface becomes saturated where no current increase could be measured above 10^{-6} molL^{-1}. The detection limit is remarkably low, reaching 2.5 × 10^{-11} mol L^{-1} (S/N = 3).

This sensor setup was also compared with SiO_2/GCE without ZnO dopants (Figure S2). A consistent DPV response could be obtained at much higher concentrations with a linear range between 5 × 10^{-7} and 2.5 × 10^{-6} molL^{-1}. ZnO doping thus enables monitoring of trace amounts of Cd^{2+} ions, while SiO_2 spheres alone are better suited for quantification of Cd^{2+} ions in highly polluted environments. By focusing on the detection of trace amounts, the advantageous properties of ZnO doping in this composite can be compared to recently reported sensors [46–56], as summarized in Table 1.

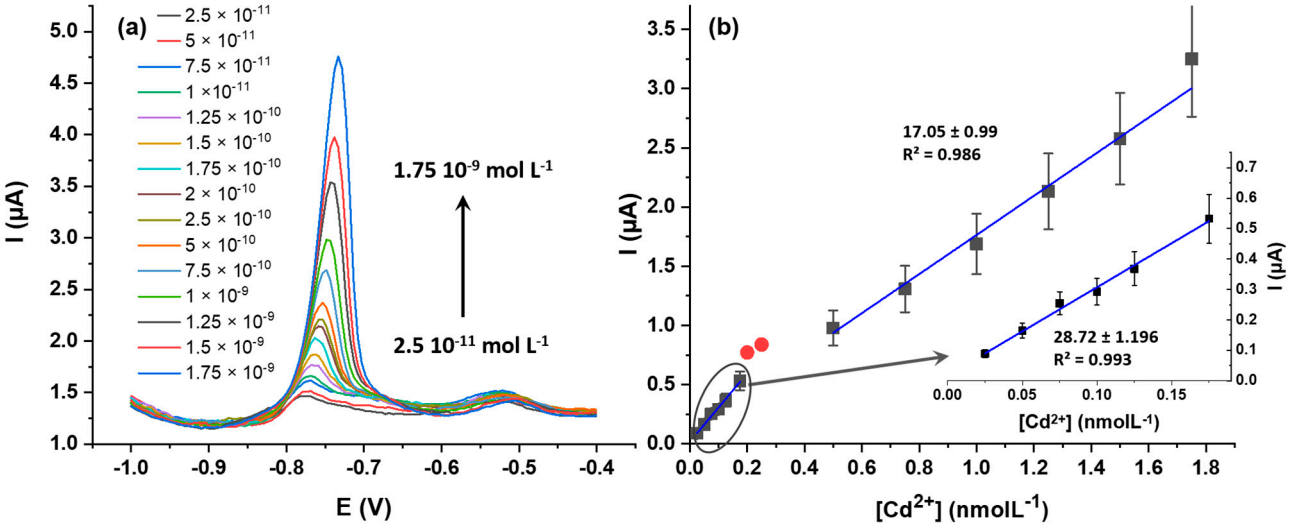

Figure 8. (**a**) Differential pulse voltammograms for Cd^{2+} at varying concentrations using a $ZnO@SiO_2$/GCE electrode in 0.1 $molL^{-1}$ ABS buffer pH 5) and (**b**) calibration curves for Cd^{2+} detection on $ZnO@SiO_2$/GCE electrodes. The concentration range between 0.2 and 0.5 $nmolL^{-1}$ (red points) are not be considered due to the change in the electrochemical Cd^{2+} oxidation process.

Table 1. Comparison of our setup with other electrochemical sensors for the determination of Cd^{2+} by DPV.

Modified Electrode	Method	Linear Range ($molL^{-1}$)	Detection Limit ($molL^{-1}$)	Reference
Chitosan-carbon nanotubes/GCE	SWASV	1.3×10^{-5}–3.9×10^{-5}	7.1×10^{-6}	[46]
LAL-AuNPs/GCE	SWASV	3.0×10^{-7}–1.4×10^{-6}	3.0×10^{-7}	[47]
Porous carbon-PdNPs/GCE	DPV	5.0×10^{-7}–5.5×10^{-6}	4.1×10^{-8}	[48]
MIL-53(Fe)/GCE	DPV	1.5×10^{-7}–4.5×10^{-7}	1.6×10^{-8}	[49]
Fe_3O_4/RGO/GCE	SWASV	0–8×10^{-7}	5.6×10^{-8}	[2]
Nano-PPCPE	DPASV	10^{-7}–3×10^{-6}	7.8×10^{-8}	[50]
PA/PPY/GO/GCE	DPV	4.4×10^{-8}–1.3×10^{-6}	1.9×10^{-8}	[51]
MSK-NPs@GRCPE	DPASV	5×10^{-11}–2×10^{-6}	5.44×10^{-9}	[52]
NH_2@GCE	DPV	3×10^{-7}–1.5×10^{-5}	2×10^{-7}	[53]
GCE/ZSM-5/Pt (5.4%)	DPV	10^{-7}–7.2×10^{-6}	1.2×10^{-9}	[54]
PPh_3/MWCNTs/IL/CPE	DPASV	1×10^{-10}–1.5×10^{-7}	7.4×10^{-5}	[55]
GCE/SBA-15/ZrO_2 (30%)	SWASV	10^{-7}–5.5×10^{-6}	3.14×10^{-7}	[56]
SiO_2/GCE	DPV	5×10^{-7}–2.5×10^{-6}	5×10^{-7}	This work
$ZnO@SiO_2$/GCE	DPV	2.5×10^{-11}–1.75×10^{-10} and 2×10^{-10}–1.75×10^{-9}	4.4×10^{-11}	This work

SWASV: square wave anodic stripping voltammetry; DPASV: differential pulse anodic stripping voltammetry; DPV: differential pulse voltammetry; LAL: laser ablation in liquid; Fe_3O_4/RGO/GCE: magnetite-reduced graphene oxide modified glassy carbon electrode; Nano-PPCPE: nanoporous pseudo carbon paste electrode; PA/PPY/GO/GCE: Phytic acid-functionalized polypyrrole–graphene oxide functionalized glassy carbon electrode.

3.2.3. Appropriateness of $ZnO@SiO_2$ for Specific Cd^{2+} Detection

The $ZnO@SiO_2$ nanocomposite was selected for the specific detection of Cd^{2+} because it has a cavity structure with suitable sizes for the investigated model ion. To evaluate the sensor efficiency, ionic species with redox potentials close to Cd^{2+}, such as Ni^{2+}, Mn^{2+}, Fe^{2+}, Co^{2+}, and Pb^{2+}, were selected and used as interfering ions. As can be seen in Figure 9, the $ZnO@SiO_2$ electrode showed a significant response current for Cd^{2+} ions at −0.78 V versus Ag/AgCl and significantly lower currents for the other divalent ions within this potential range. Only Mn^{2+} showed a good response, but the potential (−0.73 V) is clearly separated from the Cd^{2+} peak potential. In addition, a higher concentration (10^{-5} $molL^{-1}$)

was used for all tested ions than for Cd^{2+} (max. 1×10^{-9}). We further investigated possible changes in the peak currents with Cd^{2+} at different concentrations in the presence of these potentially interfering ions (Figure 9a–e). Within the concentration range between 1×10^{-9} and 1×10^{-11} molL^{-1}, the signals are well reproducible, making this setup suitable for the detection of trace Cd^{2+} in contaminated samples [57,58]. The histogram in Figure 9f confirms the good reproducibility of the sensor formation (n = 3).

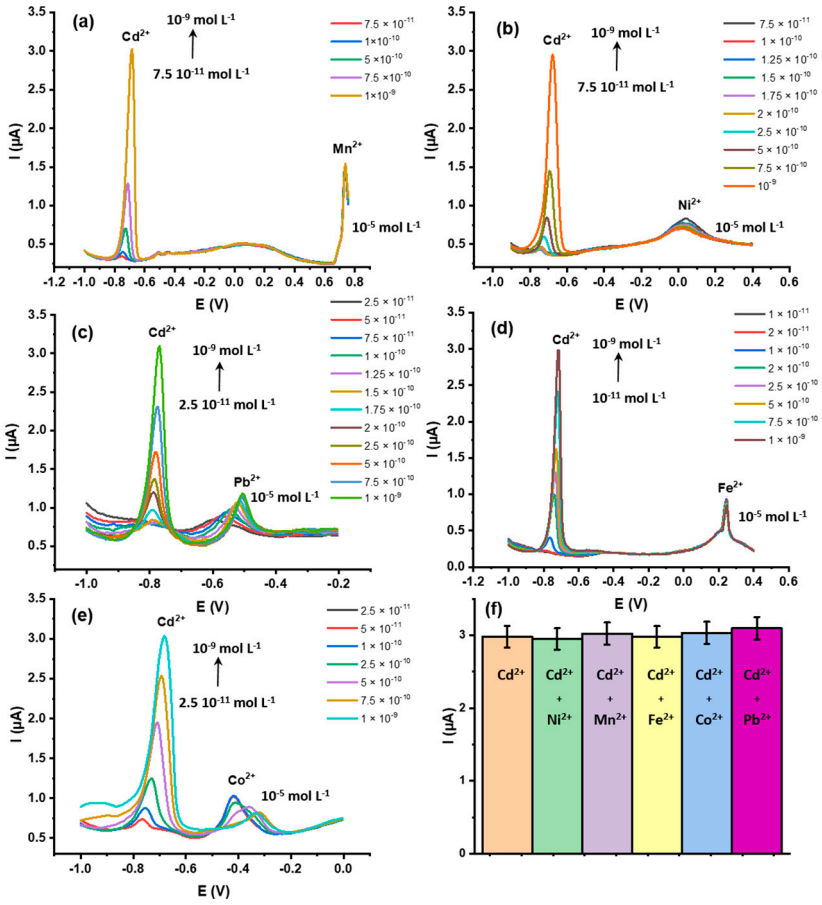

Figure 9. Differential pulse voltammograms of ZnO@SiO_2/GCE with different Cd^{2+} concentrations in the presence of potential interfering ions (**a**) Mn^{2+}, (**b**) Ni^{2+}, (**c**) Pb^{2+}, (**d**) Fe^{2+}, and (**e**) Co^{2+}). (**f**) Histogram of the maximum current peaks for Cd^{2+} at 10^{-9} molL^{-1} in the presence of the different M^{2+} ions (10^{-5} molL^{-1}). The electrodes were prepared by drop casting 7 µL of a 1 mg mL^{-1} ZnO@SiO_2 solution in ethanol, with a drying time of 2 h, and the measurements were taken with 5 min of accumulation time in 0.1 mol L^{-1} ABS buffer at pH 5.

3.2.4. Repeatability and Recovery

Repeatability and stability are crucial for the reliable performance of electrochemical sensors. Therefore, we investigated these aspects with respect to the proposed sensor. To evaluate the repeatability of ZnO@SiO_2/GCE electrodes, six different electrodes (Figure S3) coated with the same amount of the composite material were formed and subjected to DPV analysis at 10^{-9} molL^{-1} Cd^{2+} in 0.1 molL^{-1} acetate buffer (pH 5). The oxidation peak potential for Cd^{2+} was −0.78 V and the peak current showed a relative standard deviation (RSD) of 6.28%, which is still acceptable considering the low Cd^{2+} concentration (10^{-9} molL^{-1} = 8×10^{-3} µgL^{-1}) and shows the good reproducibility of the presented protocol. The repeatability of the sensor was also investigated. After Cd^{2+} determination using the DPV method (recovery cycle 0), the tested sensor was immersed in 1 molL^{-1} EDTA solution for 5 min and reconditioned for subsequent Cd^{2+} determinations (n = 4). After immersion in an aqueous EDTA solution (1 molL^{-1}), the electrode was rinsed

three times with distilled water and dried in air at room temperature for 1 h. The efficiency of this cleaning procedure is shown in Figure S4. Figure 10 shows the results of five consecutive recovery cycles using 10^{-9} molL^{-1} Cd^{2+} in a 0.1 molL^{-1} ABS buffer solution (pH 5). The current intensity decreased only slightly after the first cycle and reached 99.7% of the original peak current. The following cycles showed greater performance losses, but after five recovery cycles 95.2% could be achieved compared to the freshly manufactured electrode. These results underline the ability to reuse these electrodes several times.

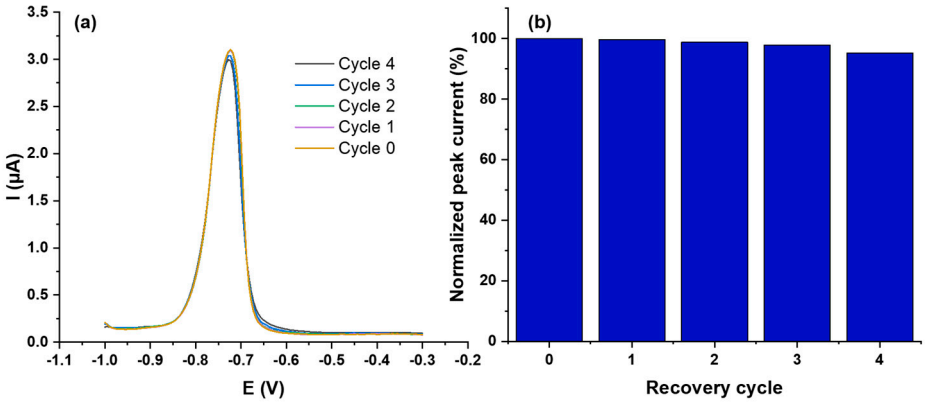

Figure 10. (**a**) DPV Sensor responses to 10^{-5} molL^{-1} of Cd^{2+} ions using one prepared ZnO@SiO_2/GCE modified electrode five times with four recovery cycles. (**b**) The resulting histogram visualizing the deviations. The measurements were taken in 1 molL^{-1} EDTA in 0.1 molL^{-1} ABS buffer at pH 5.

3.2.5. Applications to Real Samples Analysis

To test the reliability of our ZnO@SiO_2/GCE sensor, four different water samples were analyzed: tap water from the laboratory, colored water from a local store (laboratory of the textile department), seawater from Skanes, and seawater from Ksibet Elmediouni (Monastir, Tunisia). All water samples were first diluted with ABS tampon solution in a ratio of 1:99 to avoid any possible detrimental effects on the sensor performance by chloride ions. Then the samples were spiked with Cd^{2+} by diluting 1 mL of a Cd^{2+} ABS solution (1.75×10^{-6} molL^{-1}) with the corresponding volume of the real water sample to obtain the final concentration. The measured peak currents were then included in the generated calibration curve (Figure 8b) to obtain the corresponding concentration. The values obtained correlate well with the amount added, with deviations ranging from 89% (tap water) to 102% (seawater from Ksibet Elmediouni). As almost all optimized parameters (quantity, drying, and accumulation time) were met, with the exception of the pH value, these deviations are mainly due to the different pH values of the various samples (see Table 2). These results support the reliability of the proposed Cd2+ sensor for environmental water samples.

Table 2. Detection of Cd^{2+} in different environmental water sources.

Sample	Add (molL^{-1})	Found (molL^{-1})	
Tap water	1.75×10^{-9}	1.57×10^{-9}	89.71
Tinted water	1.75×10^{-9}	1.6119×10^{-9}	92
Sea water (Skanes)	1.75×10^{-9}	1.7411×10^{-9}	99.49
Sea water	1.5×10^{-9}	1.52×10^{-9}	100.66
(Ksibet Elmediouni)	1.75×10^{-9}	1.788×10^{-9}	102.2

4. Conclusions

In this study, high performance detection of Cd^{2+} was achieved using glassy carbon electrodes modified with ZnO@SiO_2 nanocomposites. DPV analysis showed that the

modification of commercial electrodes used in portable devices with this nanocomposite ($ZnO@SiO_2$) is feasible for the detection of trace amounts of Cd^{2+}. The incorporation of ZnO nanoparticles in the core significantly improved the electrochemical performance of the sensor. The experimental results showed that the electrochemical sensor using DPV transduction has good sensitivity and high selectivity. Under optimal experimental conditions, the $ZnO@SiO_2$ sensor exhibits two distinct linear ranges between 2.5×10^{-11} to 1.75×10^{-10} $molL^{-1}$ and 2×10^{-10} to 1.75×10^{-9} $molL^{-1}$, which are related to a change from diffusion-controlled to surface-controlled oxidation of Cd^{2+}. Ultimately, the $ZnO@SiO_2$ composite proved to be effective in detecting Cd^{2+} in environmental samples using DPV analysis, which enables reliable detection of Cd^{2+} in the presence of other metal ions.

Supplementary Materials: The following supporting information can be downloaded at: https://www.mdpi.com/article/10.3390/s24134179/s1, Figure S1: Optimization of experimental variables. Figure S2: Detection of Cd^{2+} with SiO_2 nanospheres. Figure S3: Repeatability studies. Figure S4: recovery of the sensor after EDTA treatment.

Author Contributions: A.D.: Investigation, Methodology, Formal Analysis, Writing—Original Draft. M.H.: Methodology, Investigation, Writing—Original Draft, Supervision. P.A.S.-C.: Methodology, Investigation, Writing—Original Draft, Supervision. S.C.: Methodology, Writing—Original Draft, Supervision. H.B.: Methodology, Formal Analysis, Supervision. All authors have read and agreed to the published version of the manuscript.

Funding: This research was funded by the Tunisian Ministry of Higher Education and Scientific Research (LR11ES55).

Institutional Review Board Statement: Not applicable.

Informed Consent Statement: Not applicable.

Data Availability Statement: All experimental data are available and can be shared on request.

Acknowledgments: The authors express their gratitude for the assistance provided by the PMIEL platform Chimie NanoBio ICMG FR 2607 (PCN-ICMG) in conducting SEM and TEM studies. Additionally, they acknowledge support from LabEx ARCANE (ANR-11-LABX-0003-01 and CBH-EUR-GS, ANR-17-EURE-0003). Special appreciation is extended to the Institut Carnot PolyNat (CARN 0007-01) for their support.

Conflicts of Interest: The authors declare no conflicts of interest.

References

1. Kubier, A.; Wilkin, R.T.; Pichler, T. Cadmium in soils and groundwater, A review. *Appl. Geochem.* **2019**, *108*, 104388. [CrossRef] [PubMed]
2. Sun, Y.F.; Chen, W.K.; Li, W.J.; Jiang, T.J.; Liu, J.H.; Liu, Z.G. Selective detection toward Cd^{2+} using Fe_3O_4/RGO nanoparticle modified glassy carbon electrode. *J. Electroanal. Chem.* **2014**, *714*, 97–102. [CrossRef]
3. Fabry, G.V.M.; Lombaert, N.; Lison, D. Dietary exposure to cadmium and risk of breast cancer in postmenopausal women: A systematic review and meta-analysis. *Environ. Int.* **2016**, *86*, 1–13. [CrossRef]
4. Bansod, B.; Kumar, T.; Thakur, R.; Rana, S.; Singh, I. A review on various electrochemical techniques for heavy metal ions detection with different sensing platforms. *Biosens. Bioelectron.* **2017**, *94*, 443–455. [CrossRef] [PubMed]
5. Farzin, L.; Shamsipur, M.; Sheibani, S. A review: Aptamer-based analytical strategies using the nanomaterials for environmental and human monitoring of toxic heavy metals. *Talanta* **2017**, *174*, 619–627. [CrossRef]
6. Motlagh, M.G.; Taher, M.A. Novel imprinted polymeric nanoparticles prepared by sol–gel technique for electrochemical detection of toxic cadmium(II) ions. *Chem. Eng. J.* **2017**, *327*, 135–141. [CrossRef]
7. Aglan, R.F.; Hamed, M.M.; Saleh, H.M. Selective and sensitive determination of Cd^{2+} ions in various samples using a novel modified carbon paste electrode. *J. Anal. Sci. Technol.* **2019**, *10*, 7. [CrossRef]
8. Komarek, J.; Krasensky, P.; Balcar, J.; Rehulka, P. Determination of palladium and platinum by electrothermal atomic absorption spectrometry after deposition on a graphite tube. *Spectrochim. Acta Part B* **1999**, *54*, 739–743. [CrossRef]
9. Guesmi, S.; Moulaee, K.; Bressi, V.; Kahri, H.; Khaskhoussi, A.; Espro, C. Houcine Barhoumi and Giovanni Neri, Non-enzymatic amperometric glucose sensing by novel Cu-MOF synthesized at room temperature. *Mater. Adv.* **2024**, *5*, 1160. [CrossRef]

10. Suturović, Z.J.; Kravić, S.Ž.; Stojanović, Z.S.; Đurović, A.D.; Brezo-Borjan, T.Ž. Potentiometric stripping analysis of cadmium and lead with constant inverse current in the analytical step using an open tubular Mercury-coated glassy carbon electrode. *J. Anal. Methods Chem.* **2019**, *8*, 3579176. [CrossRef]
11. Liu, N.; Zhao, G.; Liu, G. Coupling square wave anodic stripping voltammetry with support vector regression to detect the concentration of lead in soil under the interference of copper accurately. *Sensors* **2020**, *20*, 6792. [CrossRef] [PubMed]
12. Schurr, S.L.; Genske, F.; Strauss, H.; Stracke, A. A comparison of sulfur isotope measurements of geologic materials by inductively coupled plasma and gas source mass spectrometry. *Chem. Geol.* **2020**, *558*, 119869. [CrossRef]
13. Fang, Y.; Cui, B.; Huang, J.; Wang, L. Ultrasensitive electrochemical sensor for simultaneous determination of cadmium and lead ions based on one-step co-electropolymerization strategy. *Sens. Actuators B* **2019**, *284*, 414–420. [CrossRef]
14. Saha, D.; Barakat, S.; Van Bramer, S.E.; Nelson, K.A.; Hensley, D.K.; Chen, J. Noncompetitive and competitive adsorption of heavy metals in sulfur-functionalized ordered mesoporous carbon. *ACS Appl. Mater. Interfaces* **2016**, *8*, 34132. [CrossRef]
15. Harrington, C.F.; Clough, R.; Drennan-Harris, L.R.; Hill, S.J.; Tyson, J.F. Atomic spectrometry update. Elemental speciation. *J. Anal. At. Spectrom.* **2011**, *26*, 1561. [CrossRef]
16. Gawin, M.; Konefał, J.; Trzewik, B.; Walas, S.; Tobiasz, A.; Mrowiec, H.; Witek, E. Preparation of a new Cd (II)-imprinted polymer and its application to determination of cadmium (II) via flow-injection-flame atomic absorption spectrometry. *Talanta* **2010**, *80*, 1305–1310. [CrossRef]
17. Sarpong, K.A.; Zhang, K.; Luan, Y.; Cao, Y.; Xu, W. Development and application of a novel electrochemical sensor based on aunps and difunctional monomer-mips for the selective determination of tetrabromobisphenol-s in water samples. *Microchem. J.* **2020**, *154*, 104526. [CrossRef]
18. Kreysa, G.; Ota, K.-I.; Savinell, R.F. *Life Cycle Assessment of Sodium-Nickel-Chloride Batteries*; Springer: New York, NY, USA, 2014.
19. Hu, J.; Mao, D.; Duan, P.; Li, K.; Lin, Y.; Wang, X.; Piao, Y. Green synthesis of ZnO/BC nanohybrid for fast and sensitive detection of Bisphenol A in water. *Chemosensors* **2022**, *10*, 163. [CrossRef]
20. Walcarius, A. Mesoporous materials-based electrochemical sensors. *Electroanalysis* **2015**, *27*, 1303–1340. [CrossRef]
21. Yasri, N.G.; Gunasekaran, S. Electrochemical technologies for environmental remediation. In *Enhancing Cleanup of Environmental Pollutants*; Springer: Berlin/Heidelberg, Germany, 2017; pp. 5–73.
22. Zhang, K.; Kwabena, A.S.; Wang, N.; Lu, Y.; Cao, Y.; Luan, Y.; Liu, T.; Peng, H.; Gu, X.; Xu, W. Electrochemical assays for the detection of tbbpa in plastic products based on RGO/AgNDs nanocomposites and molecularly imprinted polymers. *J. Electroanal. Chem.* **2020**, *862*, 114022. [CrossRef]
23. Kitte, S.A.; Lia, S.; Nsabimana, A.; Gao, W.; Lai, J.; Liu, Z.; Xu, G. Stainless steel electrode for simultaneous stripping analysis of Cd (II), Pb (II), Cu (II) and Hg (II). *Talanta* **2019**, *191*, 485–490. [CrossRef] [PubMed]
24. Aravind, A.; Mathew, B. Electrochemical sensor based on nanostructured ion imprinted polymer for the sensing and extraction of Cr (III) ions from industrial wastewater. *Polym. Int.* **2018**, *67*, 1595–1604. [CrossRef]
25. Xu, W. Selective enrichment-release of trace dibutyl phthalate via molecular-imprinting based photo-controlled switching followed by high-performance liquid chromatography analysis. *J. Sep. Sci.* **2021**, *44*, 513–520.
26. Xu, W.; Gao, M.; Yin, X.; Zhang, L.; Cao, Y.; Zhang, Y.; Huang, W. Photo-stimulated "turn-on/off" molecularly imprinted polymers based on magnetic mesoporous silicon surface for efficient detection of sulfamerazine. *J. Sep. Sci.* **2020**, *43*, 2550–2557. [CrossRef] [PubMed]
27. Yang, W.; Qing, Y.; Cao, Y.; Luan, Y.; Lu, Y.; Liu, T.; Xu, W.; Huang, W.; Li, T.; Ni, X. A stimuli response, core-shell structured and surface molecularly imprinted polymers with specific pH for rapid and selective detection of sulfamethoxazole from milk sample. *React. Funct. Polym.* **2020**, *151*, 104578. [CrossRef]
28. Aravind, A.; Mathew, B. Tailoring of nanostructured material as an electrochemical sensor and sorbent for toxic Cd (II) ions from various real samples. *J. Anal. Sci. Technol.* **2018**, *9*, 22. [CrossRef]
29. Dinari, M.; Tabatabaeian, R. Ultra-fast and highly efficient removal of cadmium ions by magnetic layered double hydroxide/guar gum bio nanocomposites. *Carbohydr. Polym.* **2018**, *192*, 317–326. [CrossRef] [PubMed]
30. Xu, W.; Zhang, Y.; Yin, X.; Zhang, L.; Cao, Y.; Ni, X.; Huang, W. Highly sensitive electrochemical BPA sensor based on titanium nitride-reduced graphene oxide composite and core-shell molecular imprinting particles. *Anal. Bioanal. Chem.* **2021**, *413*, 1081–1090. [CrossRef] [PubMed]
31. Huang, W.; Zhou, X.; Luan, Y.; Cao, Y.; Wang, N.; Lu, Y.; Liu, T.; Xu, W. A sensitive electrochemical sensor modified with multiwalled carbon nanotubes doped molecularly imprinted silica nanospheres for detecting chlorpyrifos. *J. Sep. Sci.* **2020**, *43*, 954–961. [CrossRef]
32. Walcarius, A. Silica-based electrochemical sensors and biosensors: Recent trends. *Curr. Opin. Electrochem.* **2018**, *10*, 88–97. [CrossRef]
33. Cannas, C.; Mainas, M.; Musinu, A.; Piccaluga, G. ZnO/SiO_2 nanocomposites obtained by impregnation of mesoporous silica. *Compos. Sci. Technol.* **2003**, *63*, 1187–1191. [CrossRef]
34. Chireh, M.; Karam, Z.M.; Naseri, M.; Jafarinejad-Farsangi, S.; Ghaedamini, H. Synthesis, characterization and cytotoxicity study of graphene/doped ZnO/SiO_2 nanocomposites. *Appl. Phys. A* **2022**, *128*, 107. [CrossRef]
35. Castillo, J.; Arcuri, M.; Vargas, V.; Piscitelli, V. Synthesis of nanocomposites SiO_2@Co_3O_4, SiO_2@ZnO, and SiO_2@CuO from rice husks: Spectroscopy and optical properties. *Appl. Phys. A* **2022**, *128*, 107. [CrossRef]

36. Govindhan, P.; Pragathiswaran, C. Silver Nanoparticle Decorated on ZnO@SiO_2 Nanocomposite and Application for Photocatalytic Dye Degradation of Methylene Blue. *Natl. Acad. Sci. Lett.* **2019**, *42*, 323–326. [CrossRef]
37. Ali, A.M.; Harraz, F.A.; Ismail, A.A.; Al-Sayari, S.A.; Algarni, H.; Abdullah, G. Al-Sehemi. Synthesis of amorphous ZnO–SiO_2 nanocomposite with enhanced chemical sensing properties. *Thin Solid Films* **2015**, *605*, 277–282. [CrossRef]
38. Kava, A.A.; Beardsley, C.; Hofstetter, J.; Henry, C.S. Disposable glassy carbon stencil printed electrodes for trace detection of cadmium and lead. *Anal. Chim. Acta* **2020**, *1103*, 58–66. [CrossRef] [PubMed]
39. Liu, H.; Zhou, Y.; Qi, Y.; Sun, Z.; Gong, B. Preparation of thiamphenicol magnetic surface molecularly imprinted polymers for its selective recognition of thiamphenicol in milk samples. *J. Liq. Chromatogrn Relat. Technol.* **2018**, *41*, 868–879. [CrossRef]
40. Paramitha, T.; Suryadi, J.; Raissa, R.A.; Nugraha, T.A.; Utami, N. Preliminary Study of ZnO/SiO_2 Synthesis with Silica from Geothermal Solid Waste and Its Performance Test in Methylene Blue Removal. *J. Ris. Kim.* **2023**, *9*, 266–277.
41. Raevskaya, A.E.; Panasiuk, Y.V.; Stroyuk, O.L.; Kuchmiy, S.Y.; Dzhagan, V.M.; Milekhin, A.G.; Yeryukov, N.A.; Sveshnikova, L.A.; Rodyakina, E.E.; Plyusnin, V.F.; et al. Spectral and luminescent properties of ZnO–SiO_2 core–shell nanoparticles with size-selected ZnO cores. *RSC Adv.* **2014**, *4*, 63393–63401. [CrossRef]
42. Galedari, N.A.; Rahmani, M.; Tasbihi, M. Preparation, characterization, and application of ZnO@SiO_2 core–shell structured catalyst for photocatalytic degradation of phenol. *Environ. Sci. Pollut. Res.* **2017**, *24*, 12655–12663. [CrossRef]
43. Abbaa, E.; Shehub, Z.; Lamayi, D.W.; Yoriyo, K.P.; Dogara, R.K.; Ayuk, N.C. Novel developments of ZnO/SiO_2 nanocomposite: A nanotechnological approach towards insect vector control. *J. Nig. Soc. Phys. Sci.* **2021**, *3*, 262–266. [CrossRef]
44. Danbature, W.L.; Yoro, M.; Shehu, Z.; Madugu, Y.D. Solvent FreeMechanochemical Synthesis, Characterization and Antibacterial Potency of CaO/SiO_2 Nanocomposite. *J. Mater. Sci. Res. Rev.* **2019**, *4*, 1–7.
45. Fageria, P.; Gangopadhyay, S.; Pande, S. Synthesis of ZnO/Au and ZnO/Ag nanoparticles and their photocatalytic application using UV and visible light. *RSC Adv.* **2014**, *4*, 24962. [CrossRef]
46. Wu, K.H.; Lo, H.M.; Wang, J.C.; Yu, S.Y.; Yan, B.D. Electrochemical detection of heavy metal pollutant using crosslinked chitosan/carbon nanotubes thin film electrodes. *Mater. Express* **2017**, *7*, 15–24. [CrossRef]
47. Xu, X.; Duan, G.; Li, Y. Fabrication of gold nanoparticles by laser ablation in liquid and their application for simultaneous electrochemical detection of Cd^{2+}, Pb^{2+}, Cu^{2+}, Hg^{2+}. *ACS Appl. Mater. Interfaces* **2013**, *6*, 65–71. [CrossRef] [PubMed]
48. Veerakumar, P.; Veeramani, V.; Chen, S.-M.; Madhu, R.; Liu, S.-B. Palladium Nanoparticle Incorporated Porous Activated Carbon: Electrochemical Detection of Toxic Metal Ions. *ACS Appl. Mater. Interfaces* **2016**, *8*, 1061–1554. [CrossRef]
49. Tran, H.V.; Dang, H.T.M.; Tran, L.T.; Tran, C.V.; Huynh, C.D. Metal-Organic Framework MIL-53(Fe): Synthesis, Electrochemical Characterization, and Application in Development of a Novel and Sensitive Electrochemical Sensor for Detection of Cadmium Ions in Aqueous Solutions. *Adv. Polym. Technol.* **2020**, *2020*, 6279278. [CrossRef]
50. Liu, Y.; Li, T.; Ling, C.; Chen, Z.; Deng, Y.; He, N. Electrochemical sensor for Cd^{2+} and Pb^{2+} detection based on nano-porous pseudo carbon paste electrode. *Chin. Chem. Lett.* **2019**, *30*, 2211–2215. [CrossRef]
51. Dai, H.; Wang, N.; Wang, D.; Ma, H.; Lin, M. An electrochemical sensor based on phytic acid functionalized polypyrrole/graphene oxide nanocomposites for simultaneous determination of Cd^{2+} and Pb(II). *Chem. Eng. J.* **2016**, *299*, 150–155. [CrossRef]
52. Rahim, A.M.A.; Mahmoud, E.M.M. Recent advances in the modification of electrodes for trace metal analysis: A review. *Anal. Sci.* **2023**, *39*, 179. [CrossRef]
53. Yu, L.; Wan, J.W.; Meng, X.Z.; Gu, H.W.; Chen, Y.; Yi, H.C. A simple electrochemical method for Cd(II) determination in real samples based on carbon nanotubes and metal-organic frameworks. *Int. J. Environ. Anal. Chem.* **2022**, *102*, 4757. [CrossRef]
54. Tamizhdurai, P.; Rajakumaran, R.; Sakthinathan, S.; Chen, S.M.; Chiu, T.-W.; Narayanan, S. Highly sensitive detection of environmental pollutant cadmium with ultrasonic irradiated Pt-supported ZSM-5 modified electrode. *Microporous Mesoporous Mater.* **2020**, *307*, 110449. [CrossRef]
55. Bagheri, H.; Afkhami, A.; Khoshsafar, H.; Rezaei, M.; Shirzadmehr, A. Simultaneous electrochemical determination of heavy metals using a triphenylphosphine/MWCNTs composite carbon ionic liquid electrode. *Sens. Actuators B Chem.* **2013**, *186*, 451–460. [CrossRef]
56. Tamizhdurai, P.; Sakthinathan, S.; Krishnan, P.S.; Ramesh, A.; Mangesh, V.L.; Abilarasu, A.; Narayanan, S.; Shanthi, K.; Chiu, T.W. Catalytic activity of ratiodependent SBA-15 supported zirconia catalysts for highly selective oxidation of benzyl alcohol to benzaldehyde and environmental pollutant heavy metal ions detection. *J. Mol. Struct.* **2019**, *1176*, 650–661. [CrossRef]
57. Ghazali, N.N.; Mohamad Nor, N.; Abdul Razak, K.; Lockman, Z.; Hattori, T. Hydrothermal synthesis of bismuth nanosheets for modified APTES-functionalized screen-printed carbon electrode in lead and cadmium detection. *J. Nanopart. Res.* **2020**, *22*, 211. [CrossRef]
58. Kong, X.F.; Yang, B.; Xiong, H.; Zhou, Y.; Xue, S.G.; Xu, B.Q.; Wang, S.X. Selective removal of heavy metal ions from aqueous solutions with surface functionalized silica nanoparticles by different functional groups. *J. Cent. South Univ.* **2014**, *21*, 3575–3579. [CrossRef]